Dalton Transactions

ROYAL SOCIETY OF CHEMISTRY

PAPER

View Article Online
View Journal | View Issue

Cite this: *Dalton Trans.*, 2021, **50**, 10779

Electrocatalytic syngas generation with a redox non-innocent cobalt 2-phosphinobenzenethiolate complex†

Nicholas M. Orchanian, Lorena E. Hong,‡ David A. Velazquez‡ and Smaranda C. Marinescu *

Received 19th September 2020,
Accepted 13th May 2021

DOI: 10.1039/d0dt03270k

rsc.li/dalton

A cobalt complex supported by the 2-(diisopropylphosphaneyl)benzenethiol ligand was synthesized and its electronic structure and reactivity were explored. X-ray diffraction studies indicate a square planar geometry around the cobalt center with a trans arrangement of the phosphine ligands. Density functional theory calculations and electronic spectroscopy measurements suggest a mixed metal–ligand orbital character, in analogy to previously studied dithiolene and diselenolene systems. Electrochemical studies in the presence of 1 atm of CO_2 and Brønsted acid additives indicate that the cobalt complex generates syngas, a mixture of H_2 and CO, with faradaic efficiencies up to >99%. The ratios of H_2 : CO generated vary based on the additive. A H_2 : CO ratio of ~3 : 1 is generated when H_2O is used as the Brønsted acid additive. Chemical reduction of the complex indicates a distortion towards a tetrahedral geometry, which is rationalized with DFT predictions as attributable to the populations of orbitals with σ*(Co–S) character. A mechanistic scheme is proposed whereby competitive binding between a proton and CO_2 dictates selectivity. This study provides insight into the development of a catalytic system incorporating non-innocent ligands with pendant base moieties for electrochemical syngas production.

Introduction

Displacing fossil fuels in the electricity generation, transportation, and chemical production sectors with sustainable alternatives would allow for continued global advancement while mitigating the resulting environmental impact.[1,2] While sunlight provides a renewable source of energy, its spatio-temporal variability demands distributed energy storage to meet peak demands.[3] An ideal solution is to redirect excess solar-derived electricity towards electrocatalytic cells at times of low demand to convert abundant small molecules into liquid fuels and industrial chemicals.[4] Of particular interest for solar energy conversion are the fundamental reactions of photosynthesis: water splitting and CO_2 reduction.[5] Storing solar energy through the chemical transformation of these substrates offers a strategy to recycle captured CO_2.[6] Synthesis gas (syngas), a combination of CO and H_2 in ratios of 1 : 1 to 1 : 3, is a valuable feedstock derived from coal or natural gas in widescale use for the synthesis of hydrocarbons for diesel fuel (through Fischer–Tropsch chemistry) and the production of methanol.[7–10] A sustainable energy future will require a non-fossil fuel method for the formation of syngas, and the electrolysis of CO_2 using solar-derived electricity is a viable pathway to do so.[11] In particular, it is vital to develop solar-to-fuel technologies based on complexes containing only non-precious elements that catalyze water splitting and CO_2 reduction with high selectivity.[11] Fundamental studies into the electronic structure and reactivity of molecular systems offers a promising path to develop mechanistic understandings of these transformations, which may ultimately lead to new design principles.

The development of molecular catalysts allows for synthetically-tunable active sites with rapid and selective reactivity.[12,13] Numerous molecular systems have been reported for the selective conversion of CO_2 to CO, as well as for the reduction of protons to H_2.[14,15] However, fewer systems have been reported which allow for tunable generation of syngas mixtures and fewer yet which use only non-precious metals.[16] One literature example describes photoelectrocatalytic syngas production with a homogeneous rhenium bipyridine complex at a p-Si photoelectrode.[17] It is proposed that the homogeneous rhenium catalyst produces CO, while the surface of the p-Si

Department of Chemistry, University of Southern California, Los Angeles, CA, 90089, USA. E-mail: smarinesc@usc.edu

†Electronic supplementary information (ESI) available: Experimental procedures, ^{1}H NMR spectroscopy, crystallographic tables, UV-Vis data, and electrochemical data (PDF). CCDC 1985377 (CoPS), and 2081397 ([CoPS]$^-$). For ESI and crystallographic data in CIF or other electronic format see DOI: 10.1039/d0dt03270k

‡Equal contribution.

photoelectrode facilitates H_2 evolution. Single-component systems have also been reported, such as nickel and cobalt complexes, which generate tunable syngas mixtures by varying the applied potential.[18,19] A ruthenium(II) polypyridyl carbene complex was reported to facilitate both syngas production and water oxidation in aqueous media.[20] In both cases, the competitive binding of CO_2 or H^+ as substrate in the catalytic cycle was identified as a key step in determining the overall product selectivity. As such, we consider the need to include structural motifs to facilitate this competitive binding.

Ligand non-innocence and hydrogen-bonding interactions have been shown to lower the activation barrier of reactive intermediates and to direct proton-coupled electron transfer (PCET) reactions.[21] Many synthetic systems have been devised to exploit these structural motifs, in analogy to CO-dehydrogenase and [FeFe]-hydrogenase for the reversible conversion of CO_2 to CO and protons to H_2, respectively.[22–24] Thiolate and selenolate ligands in cobalt bis(dithiolene) and bis(diselenolene) complexes have been shown to serve as proton relays, proximal to a cobalt hydride, which facilitate rapid H_2 evolution.[25–28] These cobalt chalcogenide complexes have been primarily optimized for H_2 evolution over CO_2 reduction. In order to develop a system with competitive CO_2 binding, prior studies suggest that stronger donor ligands may be necessary to increase the nucleophilicity of the cobalt center.[29–31]

Hybrid phosphine–thiolate (PS) chelating systems offer both a strong σ-donor phosphine for the stabilization of low-valent metal centers as well as a π-basic thiolate ligand, which may serve to facilitate hydrogen-bond networks. It was shown that ligand protonation in a cobalt complex with thiolate and phosphine donors facilitates CO_2 reduction with high turnover frequency (1559 s^{-1}), low overpotential (70 mV), and high selectivity for CO (~95%).[32] Analogous systems based on a 2-phosphaneylbenzenethiol ligand have shown promising activity towards H_2 evolution and oxidation.[33] Electronic structure calculations of cobalt and rhenium complexes with 2-(diphenylphosphaneyl)benzenethiol ligand derivatives have indicated that this ligand platform facilitates similar orbital interactions as those facilitated by dithiolenes.[33,34] Catalytic studies of nickel and rhenium complexes supported by PS ligands have provided insight into the behavior of this ligand class, suggesting both metal-centered and ligand-centered reactivity.[33] Herein, we describe a cobalt complex supported by the 2-(diisopropylphosphaneyl)benzenethiol ligand, $[Co^{II}(P(iPr)_2SC_6H_4)_2]$, designated CoPS. Along with structural characterization, density functional theory (DFT) and time-dependent DFT calculations are explored to model the electronic structure of this system. The reactivity of CoPS is studied in the presence of CO_2 and various Brønsted acid additives, including water.

Results and discussion

Single crystal X-ray diffraction studies of CoPS indicate a square planar geometry around the cobalt center with a trans

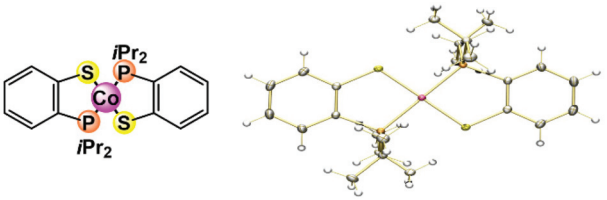

Fig. 1 Left: Chemdraw illustration of CoPS. Right: Solid state structure of CoPS, top view with the following color designations for atoms: Co = pink, S = yellow, P = orange, C = gray, H = white.

arrangement of the phosphine ligands (Fig. 1, details tabulated in Tables S1–S3†). The complex exhibits pseudo C_{2h} symmetry with eclipsed isopropyl substituents, though the orientation of these substituents may be attributed to packing interactions in the solid state. This geometry generates a sterically-crowded cobalt center with an accessible binding pocket at cobalt and sterically-accessible thiolate moieties. The trans arrangement of the phosphine ligands is consistent with a recent report of a related complex of cobalt with a (thiolato) phenylphosphine ligand derivative, as well as with that of analogous nickel and tin complexes.[33–35] To probe this structure further, DFT calculations were performed at the 6-31G(d)/PBE level of theory (see ESI† for details) to ensure convergence. The resulting optimized geometry was confirmed as a stable minimum with frequency calculations at the same level of theory. The geometry of the optimized structure is consistent with the solid-state structure observed for CoPS, and is similar to that of the analogous phenyl derivative.[34] The measured Co–S and Co–P bond lengths of 2.1625(4) and 2.2163(5) Å, respectively, are also consistent with the optimized DFT geometry. No counter-ions are observed in the outer-sphere, consistent with a neutral complex, with a single benzene solvent molecule per unit cell. Elemental analysis of the complex is also consistent with the predicted chemical formula (see Experimental methods).

^{1}H NMR spectroscopy studies of CoPS in benzene-d_6 (selected for increased solubility) reveal four broad paramagnetic resonances at δ −22.5, −16.1, 11.2, and 24.9 ppm, which each integrate to two protons and are attributed to the aromatic protons of the benzene backbone. Additional resonances at δ −0.5, 2.5, and 4.8 ppm are observed and integrate to a total of 28 protons in a 3 : 1 : 3 ratio. These resonances are assigned to the distinct isopropyl environments (Fig. S1†). The molecular nature of this complex was also confirmed in acetonitrile through NMR spectroscopy studies, which show analogous resonances in the paramagnetic spectra (Fig. S1†). Paramagnetic susceptibility measurements were performed in benzene-d_6 according to Evan's method to determine the effective magnetic moment of CoPS (see ESI†).[36] Based on these studies, a μ_{eff} of 1.77μ_B was determined, which corresponds to one unpaired electron and is consistent with the value of 2.07μ_B reported for the (thiolato)phenylphosphine derivative.[34] These results are supported by unrestricted single-point energy calculations at the def2-TZVP/PBE level of

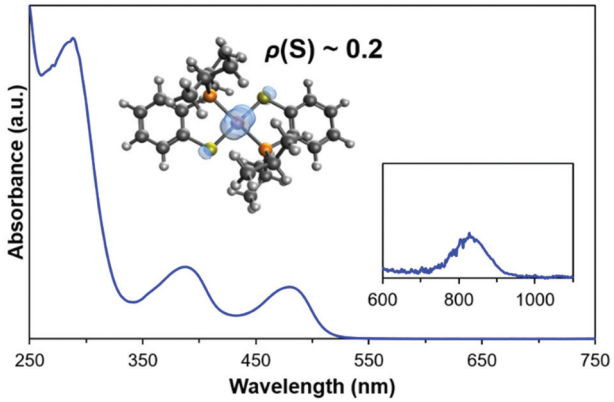

Fig. 2 Electronic spectroscopy study of 0.2 mM CoPS in a benzene solution. Inset highlights a low-energy transition at ~830 nm. Also shown is the calculated spin density for the ground state, indicating ~20% thiyl-radical character.

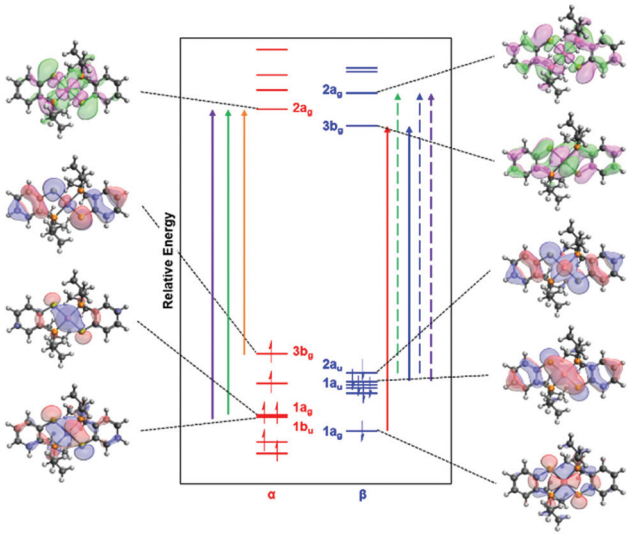

Fig. 3 Molecular orbital diagram based on TD-DFT calculations at the def2-TZVP/B3LYP level of theory. Donor orbitals shown with negative regions colored red, and positive regions colored blue, acceptor orbitals are shown with negative regions colored green, and positive regions colored pink. Vertical lines indicate major contributions (solid) and additional contributions (dashed), with transitions identified by color (λ_1 = red, λ_2 = orange, λ_3 = green, λ_4 = blue, and λ_5 = violet).

theory, which predict the neutral complex to exhibit ground state doublet character with minor spin density localized on the thiolate ligands (ρ = 0.2), suggesting some degree of thiyl-radical character as illustrated in Fig. 2 and S2.†

The electronic structure of this complex was probed experimentally through UV-Vis spectroscopy in a benzene solution. Upon dissolution in benzene, the intense orange crystals produce a vivid, yellow solution. As seen in Fig. 2, four dominant electronic transitions were observed with one additional shoulder. Dilution studies were also performed to determine the molar extinction coefficients for these transitions. The results of these studies reveal transitions at λ (ε) [nm (M^{-1} cm^{-1})] = 834 (3.8), 480 (2862.8), 388 (3975.3), 358 (2491.0, shoulder), and 288 (15 871.0) (see Fig. S3 and Table S7†). Similar spectra were recently reported for a related complex, $Co^{II}[P(Ph)_2(C_6H_3\text{-}3\text{-}SiMe_3\text{-}2\text{-}S)]_2$, which was shown to rapidly react with oxygen resulting in a change in the electronic spectrum.[34] In contrast to this prior report, the measured UV-Vis spectra for the complex reported here, CoPS, does not display a change with air exposure and all UV-Vis measurements were performed under ambient atmosphere with no color change observed in the solution. The observed electronic spectrum of the CoPS complex is also analogous to that reported for a cobalt bis(dithiolene) complex, suggesting similar electronic structure and a mixed metal–ligand ground state. As such, assignment of the oxidation state of cobalt is ambiguous, although related studies suggests a Co(II) ground state.[34] Analogous transitions were observed in acetonitrile, suggesting a coordination environment analogous to that in benzene (Fig. S17†).

To further probe the electronic structure of CoPS, unrestricted time-dependent density functional theory (TD-DFT) calculations were performed at the def2-TZVP/B3LYP level of theory in the gas phase. The B3LYP functional was selected based on literature precedent, as this functional provides an appropriate description of a broad range of molecular transition metal complexes.[37] The resulting Kohn–Sham molecular orbital picture is depicted in Fig. 3 (details tabulated in the ESI†). The predicted UV-Vis spectrum parallels the experimental spectra with five dominant transitions, though the absolute energies of these predictions vary due to the gas-phase nature of these calculations (Table S8†). As such, these calculations offer qualitative predictions for the character of the electronic transitions. Based on these calculations, the ground state electronic configuration of the complex is predicted to have a singly occupied $3b_g$ orbital, which displays π^* (Co–S) character with significant contribution from the S(p) and Co(d_{xz}) orbitals. This qualitative SOMO character parallels that predicted for both the cobalt bis(dithiolene) and bis(diselenolene) complexes.[21] The lowest-lying unoccupied one-electron orbital corresponds to the $3b_g$ β orbital, which exhibits similar character as the α SOMO with more substantial metal contribution.

As illustrated in Fig. 3, the lowest-energy transition observed at 834 nm (λ_1) is predicted to correspond to the singlet-to-singlet excitation of a β spin in an orbital of a_g symmetry with Co(d_{xy}) and S(p_y) orbital contribution to the mixed metal–ligand $3b_g$ orbital. The next lowest-energy transition (λ_2 = 480 nm) is predicted to correspond to a ligand-to-metal charge transfer (LMCT) excitation of an α electron from the $3b_g$ mixed metal–ligand character SOMO with predominant ligand-character to the $2a_g$ LUMO, which exhibits σ*(Co–S) character with contributions from S(p_x) and Co($d_{x^2-y^2}$) orbitals. The electronic transition observed at 388 nm (λ_3) is predicted to exhibit metal-to-ligand charge transfer (MLCT) character with both α and β contribution. An additional shoulder appearing at 358 nm (λ_4) is attributed to excitation of an electron from occupied orbitals with S(p_z) and Co(d_{z^2}) contribution to the $2a_g$ LUMO. Finally, the highest-energy observed tran-

sition (λ_5 = 288 nm) is predicted to correspond to a ligand-to-metal charge transfer (LMCT) transition from the $1b_u$ orbital exhibiting $S(p_y)$ contributions to the $2a_g$ LUMO of $Co(d_{x^2-y^2})$ character.

The electrochemical behavior of CoPS was analyzed by cyclic voltammetry (CV) studies in an acetonitrile solution with 0.1 M [nBu$_4$N][PF$_6$] electrolyte using a glassy carbon working electrode (3 mm diameter).[38] Acetonitrile was selected as the electrochemical solvent in analogy to the studies performed on the cobalt bis(dithiolene) and bis(diselenolene) complexes. Under N_2 atmosphere, the complex displays a reversible one-electron oxidation feature with $E_{1/2}$ at −0.21 V, and two quasi-reversible reductive features at −2.08 V, and −2.36 V, respectively (Fig. 4 and Fig. S4†). All potentials are referenced *versus* $Fc^{0/+}$ and the reversibility and one-electron nature of these features is based on comparison to the internal $Fc^{0/+}$ reference. The features at −2.08 V and −2.36 V appear as quasi-reversible and one-electron waves, and no change in the reduction event at −2.08 V is observed if the potential is reversed before reaching the second reduction (Fig. S4†). While the features at −0.21 V and −2.08 V are similar in magnitude, the feature at −2.36 V is diminished indicating less charge passed (Fig. S4†). This observation suggests the formation of a minor species following the reduction event at −2.08 V, which is subsequently further reduced at −2.36 V. Based on the predicted molecular orbital diagram (Fig. 3), the anodic feature at −0.21 V is assigned to the one-electron oxidation of CoPS to $[CoPS]^+$, which results in the depopulation of the mixed metal–ligand SOMO. Following this event, the cathodic feature at −2.08 V is assigned to the one-electron reduction of CoPS to $[CoPS]^-$, resulting in a diamagnetic complex with the occupation of the mixed metal–ligand β LUMO level. The complex behavior observed for the feature at −2.36 V can be rationalized by the predicted character of the next-lowest lying orbital for the square planar configuration of CoPS. As shown in Fig. 3, a two-electron reduction of CoPS to $[CoPS]^{2-}$ is predicted to result in the occupation of an α orbital with σ*(Co–S) character. The population of this orbital can be expected to result in a change in geometry at the cobalt center, possibly leading to metal–ligand bond elongation, bond cleavage, or torsion away from a square planar coordination environment. In a related example, a square planar Co(II) complex with a (thiolato)phenylphosphine ligand derivative was shown to result in a tetrahedral coordination environment around the Co(II) center following oxidation in air.[34] The cathodic feature at −2.36 V can be tentatively assigned to the one-electron reduction of the species resulting from this reduction-initiated structural change.

To further probe the electrochemical behavior of this system, cyclic voltammetry experiments were performed at various scan rates (Fig. 5). The feature at −0.21 V appears reversible at all scan rates, and the Randles–Sevcik analysis is consistent with that of a freely diffusing molecular species (see Fig. S5†). More complex behavior is observed for the subsequent two events at −2.08 V and −2.36 V. At low scan rates, both reduction events are irreversible (see Fig. 5). Increasing the scan rate causes the first feature (at −2.08 V) to exhibit reversibility, while diminishing the second redox event. As this behavior is consistent scan-to-scan, it is unlikely to be attributable to deposition of a heterogeneous species onto the electrode surface and instead suggests that a structural change follows the one-electron reduction of CoPS. If this structural change occurs on a slower timescale than that of the CV experiment, the appearance of the peak at −2.36 V would be expected to diminish. Scan-rate dependence studies reveal that the feature at −2.36 V approaches the magnitude of the features at −0.21 V and −2.08 V as the scan rate is decreased, consistent with a structural change on a timescale competitive with that of the CV sweep. As the scan rate is decreased, more time is allowed for the generation of a new species and for the subsequent reduction of this species at −2.36 V to be detected as a feature in the CV profile. An additional oxidation feature appears at −0.56 V following reduction, further indicating the formation of a new species following reduction of the complex.

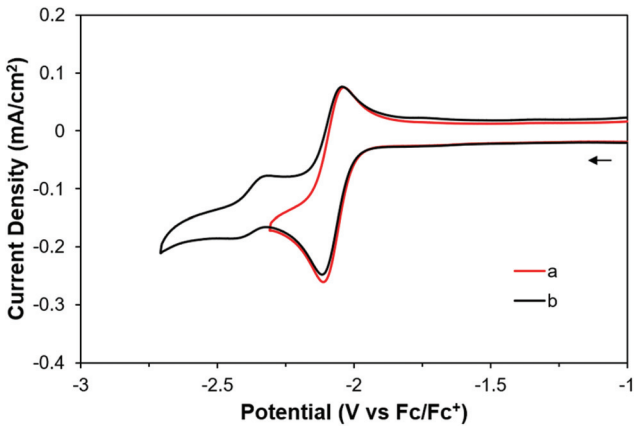

Fig. 4 Cyclic voltammograms of 1 mM CoPS in an acetonitrile solution under N_2 atmosphere with 0.1 M [nBu$_4$N][PF$_6$] with scan rate = 100 mV s^{-1}, where a represents the initial scan, and b corresponds to the subsequent scan.

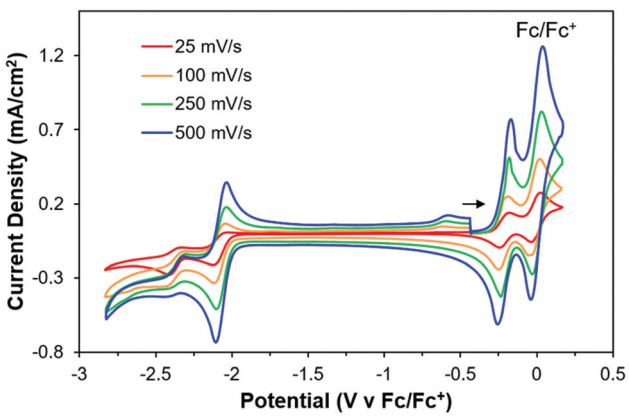

Fig. 5 Cyclic voltammograms of 1 mM CoPS in an acetonitrile solution under N_2 atmosphere with 0.1 M [nBu$_4$N][PF$_6$] and 1 mM ferrocene at various scan rates.

To understand the observed electrochemical behavior, gas-phase geometry optimizations were performed at the 6-31G(d)/PBE level of theory for the one- and two-electron-reduced forms of the complex (see ESI† for details). The one-electron reduced form, $[CoPS]^{-}$, is predicted to be diamagnetic with a singlet ground state and distorts towards a tetrahedral geometry upon relaxation, as shown in Fig. 6. This result indicates that a change in coordination geometry of the complex is predicted to be more energetically favorable than metal–ligand bond elongation in a square planar geometry or metal–ligand bond cleavage. Recent computational studies have shown that the related (thiolato)phenylphosphine derivative similarly undergoes a change in coordination geometry from square planar to tetrahedral upon addition of O_2, providing some additional support for a geometry change towards a tetrahedral structure.[34] Following this reduction, an additional one-electron reduction generates the doubly-anionic species, $[CoPS]^{2-}$, which is predicted to be paramagnetic with a doublet ground state. This complex distorts further towards a tetrahedral geometry, and the spin density for this species is predicted to localize predominantly on the metal center (Fig. S6†). Based on these calculations, the quasi-reversibility of the observed reduction features is attributed to this structural change from a square planar geometry towards a tetrahedral geometry at the cobalt center. Further, the localization of spin density predicted by DFT for the reduced species suggests that the first reduction ($E_{1/2}$ = −2.08 V) has mixed metal- and ligand-based character, while the second reduction event ($E_{1/2}$ = −2.36 V) appears to predominantly have metal-based character.

To confirm the DFT predictions, chemical reduction of CoPS with excess potassium graphite (KC_8) was performed and crystals suitable for single crystal X-ray diffraction studies were prepared though vapor diffusion of pentane into a THF solution of the reduced complex (see ESI† for details). The resulting red needles were mounted under N_2 atmosphere with care to prevent exposure to O_2. As shown in Fig. 7, single crystal diffraction studies indicate a pseudo-tetrahedral geometry

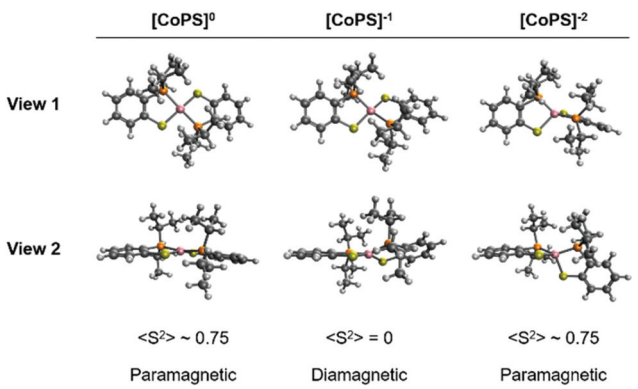

Fig. 6 Calculated geometries for $[CoPS]^{0}$, $[CoPS]^{-}$, and $[CoPS]^{2-}$ at the 6-31G(d)/PBE level of theory. All geometries were confirmed as stable minima with frequency calculations at the same level of theory.

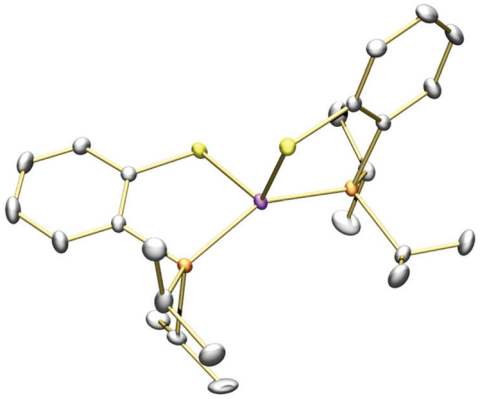

Fig. 7 Solid state structure of $[CoPS]^{-}$ with the following color designations for atoms: Co = pink, S = yellow, P = orange, C = gray, H = white. The coordinating cation (K^{+}) and hydrogen atoms are omitted for clarity.

around the cobalt center with a S(1)–Co(1)–S(2) angle of 115.93° and a P(1)–Co(1)–P(2) angle of 149.82° (Tables S4–S6†). The measured Co–S and Co–P bond lengths of 2.3161(6) and 2.2203(7) Å, respectively, indicate elongation of these bonds upon reduction (Table S5†). In particular, the Co–S bond length displays a larger elongation upon reduction, from 2.1625(4) to 2.3161(6) Å, whereas the Co–P bond length changes only from 2.2163(5) to 2.2203(7) Å. Additionally, the measured S(1)–Co(1)–S(2) and P(1)–Co(1)–P(2) angles deviate from the ideal 109.5° for tetrahedral complexes, attributed to steric crowding of the close-approaching isopropyl groups (Table S6†). The structural parameter $\tau_{[CoPS]^{-}}$ = 0.67, indicates that the one-electron reduced complex displays a cobalt coordination environment that is closer to a tetrahedral configuration rather than square planar (see ESI† for details). The structural parameter for CoPS is much closer to zero (τ_{CoPS} = 0.03), as expected for a square planar geometry. These results are consistent with the DFT predictions, and suggest that the reduction of CoPS indeed results in a distortion away from the square planar geometry of the neutral complex due to population of orbitals with σ*(Co–S) character.

The catalytic behavior of the CoPS complex was studied *via* CV experiments in the presence and absence of CO_2 and various proton donors. Upon switching the atmosphere from N_2 to CO_2, an irreversible increase in current density is observed at a potential corresponding to the first reduction event for CoPS ($E_{1/2}$ = −2.08 V), as shown in Fig. 8 and Fig. S7.† This behavior suggests reduction-induced reactivity with CO_2 rather than a pre-association of the complex with CO_2 as no shift in the onset potential is observed upon addition of CO_2. Scanning to more negative potentials reveals a pseudo-plateau shape at −2.18 V. On the return scan, a small return oxidation feature is present at −1.58 V. This return feature does not appear under N_2 alone, which suggests that it may indicate the oxidation of an intermediate in the CO_2 reduction cycle. As generation of CO from CO_2 requires two equivalents of protons, CV experiments were performed in the presence of acid additives under CO_2 atmosphere. Larger current densities

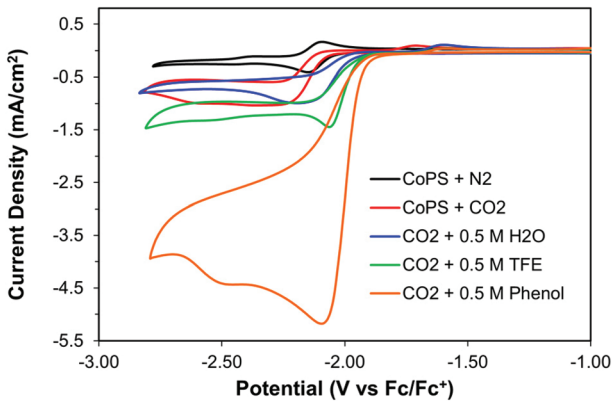

Fig. 8 Cyclic voltammograms of 1 mM CoPS in acetonitrile solutions with 0.1 M [nBu$_4$N][PF$_6$] and scan rate = 100 mV s^{-1} under N_2 (black), CO_2 (red), and under CO_2 in the presence of either 0.5 M PhOH (orange), 0.5 M TFE (green), or 0.5 M H_2O (blue).

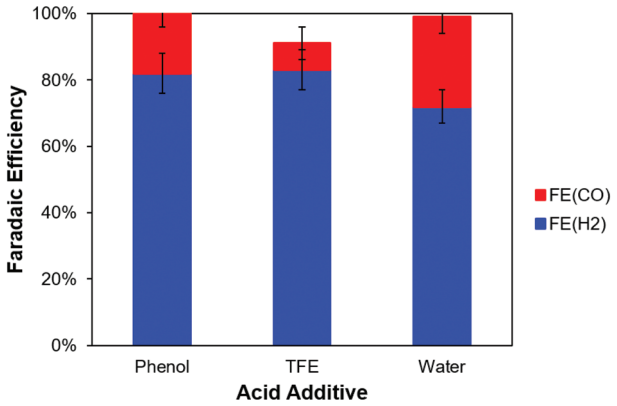

Fig. 9 Summary of CPE results illustrating faradaic efficiencies for H_2 (blue) and CO (red) production.

are measured in the presence of Brønsted acid additives, including phenol (PhOH), 2,2,2-trifluoroethanol (TFE), or H_2O (Fig. 8). While experiments in the presence of H_2O exhibit a pseudo-plateau shape at 100 mV s^{-1}, peaks are observed prior to a pseudo-plateau region in the presence of 0.5 M TFE or PhOH. This pseudo-plateau region has previously been attributed to entering a kinetic regime.[39] To further probe the behavior of this complex in the presence of CO_2, variable scan rate experiments were conducted in the absence of an acid additive. These studies indicate a change in waveshape from a plateau shape to a peak shape (see Fig. S8†) at faster scan rates. This behavior suggests an "EC"-type mechanism, where a chemical step (C) follows an electrochemical reduction step (E) and has insufficient time to proceed as the scan rate increases. This result further suggests that pre-association of CO_2 to the neutral CoPS complex (a "CE"-type mechanism) is unlikely, as a reduction event precedes a chemical step in the presence of CO_2.

Following CV studies, controlled potential electrolysis (CPE) experiments were performed with CoPS under N_2 and CO_2 atmosphere to determine product selectivity. Results for these studies are summarized in Table 1 and Fig. 9 (full tabulations provided in Tables S9–S12†). In a typical experiment, a glassy carbon working electrode was held at a potential of −2.18 V for one hour in a 1 mM solution of CoPS. A sample of the headspace was collected *via* syringe and analyzed by gas chromatography for gaseous products. Under CO_2 atmosphere in the absence of an acid additive, a stable current density of 1.1 mA cm^{-2} was measured for the duration of the experiment. Neither H_2 nor CO were detected. Detection analyses of other common CO_2-reduction products, such as formate, oxalate, methane, methanol, carbonate, and other organics (acids or aldehydes) were performed in the post-electrolysis solution and working compartment headspace, but none were detected by either NMR spectroscopy or gas chromatography measurements. Previous studies of an analogous nickel complex with both thiolate and phosphine donors suggest reduction-initiated decomposition may proceed in the absence of substrate.[40] Additionally, no products were detected for the CoPS complex under N_2 in the absence of an acid additive.

Table 1 Summary of results from CPE studies

Acid	Total FE (%)	H_2 : CO	i_{CPE}[a] (mA cm^{-2})
None	—	—	1.1
PhOH	>99	4.1 ± 0.5	4.8
TFE	91 ± 9	10.2 ± 1	2.9
H_2O	>99	2.7 ± 0.3	1.6

[a] Average current density measured over 1 hour.

In the presence of Brønsted acid additives (PhOH, TFE, or H_2O), increased electrolysis currents were measured with a concurrent increase in the quantity of the gaseous products and relatively stable total FE. The addition of 0.5 M PhOH generates a stable current density of 4.8 mA cm^{-2} (Fig. S9† and Table 1). A H_2 : CO ratio of 4.1 ± 0.5 was measured in the presence of phenol, with a total FE of >99% (Table 1 and Fig. 9). In the presence of 0.5 M TFE, an average current density of 2.9 mA cm^{-2} was observed, with a H_2 : CO ratio of 10.2 ± 1 and a total FE of 91 ± 9%. Upon addition of 0.5 M H_2O, a current density of 1.6 mA cm^{-2} was measured with a total FE of >99% and a H_2 : CO ratio of 2.7 ± 0.3.

It was observed that the choice in Brønsted acid impacts both the measured TON and the H_2 : CO ratio of the resulting syngas mixture, with the highest preference for CO production measured in the presence of H_2O (Fig. 9 and S10†). Additionally, the high FE and favorable H_2 : CO ratio measured with water was maintained for a 3-hour CPE experiment (Tables S9 and S10†). This time-dependent product quantification indicates negligible change in the H_2 : CO ratio, as both the 1 hour and 3 hours measurements in the presence of water generate H_2 : CO ratios that are within the experimental error. Neither H_2 nor CO was detected in the absence of catalyst, and no formate or oxalate or additional products (including methane, methanol, carbonate, or other organics) were

detected under any of the conditions studied (see ESI†). As the total FE is near unity in the CPE experiments performed in the presence of CoPS complex, CO_2 and Brønsted acid additives (PhOH, TFE, or H_2O), the absence of additional side products is consistent with the quantities of H_2 and CO detected. No H_2 or CO was detected in the CPE experiments performed in the presence of CoPS complex under N_2 atmosphere, and upon the addition of acid only H_2 was detected in all cases (Fig. S11 and Tables S11, S12†). Cyclic voltammetry under N_2 in the presence and absence of acid confirms that a sharp onset is observed at the $CoPS^{-/0}$ couple, consistent with H_2 evolution at these large overpotentials (Fig. S12†). Additionally, higher current densities were generated in the presence of CoPS complex and an acid additive under N_2 relative to the currents measured under CO_2 atmosphere, as indicted in Fig. S12 and S13,† respectively. This suggests a competition exists between CO_2 coordination and protonation, which hinders the hydrogen evolution reaction (HER) in the presence of CO_2. A decrease was observed in the electrolysis current density in the presence of 0.5 M PhOH under N_2, which had not been detected under CO_2 atmosphere (Fig. S11†). Cyclic voltammetry before and after electrolysis under these conditions indicates no change in the $CoPS^{0/+}$ couple at −0.21 V, suggesting that the current drop is likely associated with depletion of PhOH at these high catalytic current densities (>18 mA cm^{-2}) (Fig. S14†). Similarly, no change in the $CoPS^{0/+}$ couple at −0.21 V was observed under catalytic conditions in the presence of CO_2, further suggesting that the current drop observed under N_2 is not associated with a change in the catalyst (Fig. S13†). Rinse tests were performed following each experiment to confirm that the solubilized complex is responsible for the observed activity (Fig. S15, further details provided in ESI†). Additional control experiment studies were performed in the absence of catalyst, such as CVs conducted with a glassy carbon electrode and acid additives under N_2. These studies display low current densities for H_2O and TFE, or a sharp onset for PhOH, consistent with low background activity for hydrogen evolution by the glassy carbon working electrode at the operating potential of catalysis (Fig. S16†).

Based on the experimental observations, mechanistic pathways can be constructed to model the measured reactivity, as shown in Scheme 1. Based on the electrochemical studies, no reactivity is observed between CO_2 and CoPS prior to reduction, suggesting that an initial CO_2-binding step to the neutral species is unfavorable. In contrast, a color change from yellow to green was observed upon treatment of an acetonitrile solution of CoPS with trifluoroacetic acid (TFA), with a corresponding return to the original UV-Vis spectrum upon the addition of triethylamine base (Fig. S17†). This result suggests that the neutral complex may undergo reversible protonation prior to reduction. As TFA is a reasonably strong acid, with a pK_a of 12.8 in acetonitrile, ^{1}H-NMR spectra were collected in acetronitrile-d_3 in the presence of 0.5 M phenol, TFE, and H_2O to test whether protonation is facilitated by these acids (Fig. S18†). In the presence of 0.5 M TFE, additional paramagnetic resonances are observed at δ −18.5, −29.9, and

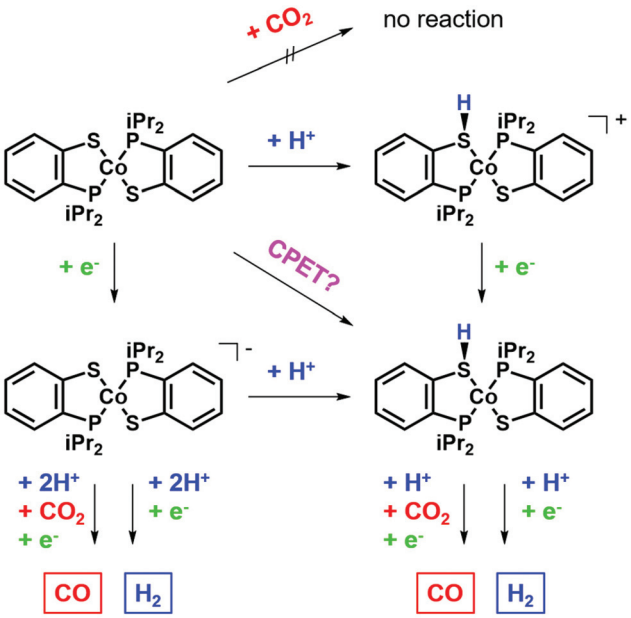

Scheme 1 Possible mechanistic paths for observed reactivity.

−56.8 ppm, attributed to the formation of protonated species, along with the resonances of the CoPS complex. These results indicate that the CoPS complex and the proposed protonated species are in equilibrium under these conditions. As these resonances are not observed in the presence of phenol or H_2O, the results of this study suggest that only TFE is capable of protonating the neutral complex prior to reduction. These results are consistent with the measured H_2 : CO ratios as TFE is observed to generate the highest H_2 : CO ratio of 10.2 ± 1. Due to the literature precedent established for cobalt bis(dithiolene) and bis(diselenolene) catalysts, we propose that this protonation event takes place at the thiolate ligand. This is further predicted by our DFT results, which indicate non-negligible thiyl-radical character. The presence of stronger acids is expected to follow this protonation-first pathway ("CE"-type mechanism), while weaker acids may follow a reduction-first pathway ("EC"-type mechanism). As such, multiple competing mechanistic pathways may be available. As CPE studies are conducted at a lower potential than the second reduction of the complex, a second reduction step (E) prior to chemical step (C) is ruled out, further suggesting EC- rather than EE-type activation. Following reduction of the neutral complex, a competition exists between CO_2-adduct formation and protonation. This step is expected to determine the overall selectivity of the catalyst, as binding of either substrate (CO_2 or protons) allows the catalyst to enter either the CO_2-reduction reaction (CO_2RR) or HER cycles. Following liberation of CO or H_2 to regenerate the neutral species, the complex can either receive another electron to regenerate the reduced complex or react with protons to regenerate the protonated species.

The overpotential for the two-electron reduction of CO_2 to CO in acetonitrile is determined based on our applied poten-

tial of −2.18 V and the reported thermodynamic potential for CO_2 reduction in the presence of various acid additives with the reported pK_a values (Table S13†).[41] As carbonic acid is formed by the reaction of CO_2 with water, the overpotential (η) for CO_2 reduction in the presence of carbonic acid is also provided for comparison. Additionally, the operation of concerted proton-coupled electron transfer pathways is suggested by cyclic voltammetry studies, and more complex mechanistic schemes are therefore likely contributing to the observed reactivity. Ongoing stoichiometric studies are underway to elucidate these competing pathways.

Conclusions

In conclusion, we report here a cobalt bis(2-[diisopropylphosphaneyl]benzenethiol) complex, CoPS, exhibiting ligand-non innocence and activity towards electrocatalytic syngas production. Electronic structure calculations predict non-negligible ground state thiyl-radical character, and electronic spectroscopy reveals a low-energy charge transfer transition. In the presence of 0.5 M phenol, the highest catalytic activity is observed with FE of >99%, and H_2 : CO ratio of 4.1 ± 0.5. Excellent FE (>99%) and a favorable H_2 : CO ratio (2.7 ± 0.3) were also measured for the co-electrolysis of CO_2 and H_2O. Possible mechanistic pathways are proposed, in which pK_a-dependent protonation by the external acid and competitive binding between CO_2 and protons determines overall selectivity, supported by cyclic voltammetry and electrolysis studies. More specifically, we propose that protonation at the sulfur site is feasible, as has been proposed for cobalt bis(dithiolate) and bis(diselenolate) systems, and that this protonation is dependent on the pK_a of the external acid, as well as the steric influence of the isopropyl substituents. This protonation may subsequently influence the binding affinity of CO_2 at the metal center.

Conflicts of interest

The authors declare no competing financial interests.

Acknowledgements

This work was supported by the U. S. Department of Energy, Office of Basic Energy Sciences, Division of Chemical Sciences, Geosciences and Biosciences under award DE-SC0019236. L. E. H. gratefully acknowledges the Rose Hills Foundation for an undergraduate research fellowship. NMR data was collected with instrumentation provided by the USC Center of Excellence for Molecular Characterization. Crystallographic data was collected with instrumentation provided by the USC Department of Chemistry X-ray Crystallographic Facility. Density functional theory calculations were performed with computational resources offered by the USC Center for Advanced Research Computing. We thank Prof. Jahan M. Dawlaty and Prof. Ralf Haiges for discussions, and Thomas Saal for assistance with single crystal X-ray diffraction studies.

References

1 IEA, *2018 World Energy Outlook: Executive Summary*, Oecd/Iea, 2018, p. 11.
2 D. G. Nocera, Solar Fuels and Solar Chemicals Industry, *Acc. Chem. Res.*, 2017, **50**, 616–619.
3 R. J. Detz, J. N. H. Reek and B. C. C. Van Der Zwaan, The Future of Solar Fuels: When Could They Become Competitive?, *Energy Environ. Sci.*, 2018, **11**, 1653–1669.
4 R. L. House, N. Y. M. Iha, R. L. Coppo, L. Alibabaei, B. D. Sherman, P. Kang, M. K. Brennaman, P. G. Hoertz and T. J. Meyer, Artificial Photosynthesis: Where Are We Now? Where Can We Go?, *J. Photochem. Photobiol., C*, 2015, **25**, 32–45.
5 D. Kim, K. K. Sakimoto, D. Hong and P. Yang, Artificial Photosynthesis for Sustainable Fuel and Chemical Production, *Angew. Chem., Int. Ed.*, 2015, **54**(11), 3259–3266.
6 C. Graves, S. D. Ebbesen, M. Mogensen and K. S. Lackner, Sustainable Hydrocarbon Fuels by Recycling CO_2 and H_2O with Renewable or Nuclear Energy, *Renewable Sustainable Energy Rev.*, 2011, **15**, 1–23.
7 U.S. Energy, *Information Administration – EIA. "New Methanol Plants Expected to Increase Industrial Natural Gas Use through 2020"*, 2019, https://www.eia.gov/.
8 G. A. Olah, Beyond Oil and Gas: The Methanol Economy, *Angew. Chem., Int. Ed.*, 2005, **44**, 2636–2639.
9 J. R. Rostrup-Nielsen, Production of Synthesis Gas, *Catal. Today*, 1993, **18**, 305–324.
10 J. Qiao, Y. Liu, F. Hong and J. Zhang, A Review of Catalysts for the Electroreduction of Carbon Dioxide to Produce Low-Carbon Fuels, *Chem. Soc. Rev.*, 2014, **43**, 631–675.
11 B. Su, Z.-C. Cao and Z.-J. Shi, Exploration of Earth-Abundant Transition Metals (Fe, Co, and Ni) as Catalysts in Unreactive Chemical Bond Activations, *Acc. Chem. Res.*, 2015, **48**, 886–896.
12 J. P. Collin and J. P. Sauvage, Electrochemical Reduction of Carbon Dioxide Mediated by Molecular Catalysts, *Coord. Chem. Rev.*, 1989, **93**, 245–268.
13 J. M. Barlow and J. Y. Yang, Thermodynamic Considerations for Optimizing Selective CO_2 Reduction by Molecular Catalysts, *ACS Cent. Sci.*, 2019, **5**, 580–588.
14 C. D. Windle and R. N. Perutz, Advances in Molecular Photocatalytic and Electrocatalytic CO_2 Reduction, *Coord. Chem. Rev.*, 2012, **256**, 2562–2570.
15 R. Francke, B. Schille and M. Roemelt, Homogeneously Catalyzed Electroreduction of Carbon Dioxide - Methods, Mechanisms, and Catalysts, *Chem. Rev.*, 2018, **118**, 4631–4701.
16 X. Zhou, D. Micheroni, Z. Lin, C. Poon, Z. Li and W. Lin, Graphene-Immobilized fac-Re(Bipy)$(CO)_3$Cl for Syngas Generation from Carbon Dioxide, *ACS Appl. Mater. Interfaces*, 2016, **8**, 4192–4198.

17 B. Kumar, J. M. Smieja, A. F. Sasayama and C. P. Kubiak, Tunable, Light-Assisted Co-Generation of CO and H_2 from CO_2 and H_2O by Re(Bipy-tBu)$(CO)_3$Cl and p-Si in Non-Aqueous Medium, *Chem. Commun.*, 2012, **48**, 272–274.

18 (*a*) J. W. Wang, H. H. Huang, J. K. Sun, D. C. Zhong and T. B. Lu, Syngas Production with a Highly-Robust Nickel(II) Homogeneous Electrocatalyst in a Water-Containing System, *ACS Catal.*, 2018, **8**, 7612–7620; (*b*) N. Elgrishi, M. B. Chambers, V. Artero and M. Fontecave, Terpyridine Complexes of First Row Transition Metals and Electrochemical Reduction of CO_2 to CO, *Phys. Chem. Chem. Phys.*, 2014, **16**, 13635–13644.

19 J. D. Froehlich and C. P. Kubiak, Homogeneous CO_2 Reduction by Ni(Cyclam) at a Glassy Carbon Electrode, *Inorg. Chem.*, 2012, **51**, 3932–3934.

20 (*a*) Z. Chen, J. J. Concepcion, M. K. Brennaman, P. Kang, M. R. Norris, P. G. Hoertz and T. J. Meyer, Splitting CO_2 into CO and O_2 by a Single Catalyst, *Proc. Natl. Acad. Sci. U. S. A.*, 2012, **109**, 15606–15611; (*b*) P. Kang, Z. Chen, A. Nayak, S. Zhang and T. J. Meyer, Single Catalyst Electrocatalytic Reduction of CO_2 in Water to H_2 + CO Syngas Mixtures with Water Oxidation to O_2, *Energy Environ. Sci.*, 2014, **7**, 4007–4012; (*c*) Z. Chen, P. Kang, M. T. Zhang and T. J. Meyer, Making Syngas Electrocatalytically Using a Polypyridyl Ruthenium Catalyst, *Chem. Commun.*, 2014, **50**, 335–337.

21 R. Eisenberg and H. B. Gray, Noninnocence in Metal Complexes: A Dithiolene Dawn, *Inorg. Chem.*, 2011, **50**, 9741–9751.

22 H. Ogata, K. Nishikawa and W. Lubitz, Hydrogens Detected by Subatomic Resolution Protein Crystallography in a [NiFe] Hydrogenase, *Nature*, 2015, **520**, 571–574.

23 A. Chapovetsky, T. H. Do, R. Haiges, M. K. Takase and S. C. Marinescu, Proton-Assisted Reduction of CO_2 by Cobalt Aminopyridine Macrocycles, *J. Am. Chem. Soc.*, 2016, **138**, 5765–5768.

24 E. M. Nichols, J. S. Derrick, S. K. Nistanaki, P. T. Smith and C. J. Chang, Positional Effects of Second-Sphere Amide Pendants on Electrochemical CO_2 Reduction Catalyzed by Iron Porphyrins, *Chem. Sci.*, 2018, **9**, 2952–2960.

25 W. R. McNamara, Z. Han, C.-J. Yin, W. W. Brennessel, P. L. Holland and R. Eisenberg, Cobalt-Dithiolene Complexes for the Photocatalytic and Electrocatalytic Reduction of Protons in Aqueous Solutions, *Proc. Natl. Acad. Sci. U. S. A.*, 2012, **109**, 15594–15599.

26 K. J. Lee, B. D. McCarthy, E. S. Rountree and J. L. Dempsey, Identification of an Electrode-Adsorbed Intermediate in the Catalytic Hydrogen Evolution Mechanism of a Cobalt Dithiolene Complex, *Inorg. Chem.*, 2017, **56**, 1988–1998.

27 C. S. Letko, J. A. Panetier, M. Head-Gordon and T. D. Tilley, Mechanism of the Electrocatalytic Reduction of Protons with Diaryldithiolene Cobalt Complexes, *J. Am. Chem. Soc.*, 2014, **136**, 9364–9376.

28 C. A. Downes, J. W. Yoo, N. M. Orchanian, R. Haiges and S. C. Marinescu, H_2 Evolution by a Cobalt Selenolate Electrocatalyst and Related Mechanistic Studies, *Chem. Commun.*, 2017, **53**, 7306–7309.

29 M. S. Jeletic, M. L. Helm, E. B. Hulley, M. T. Mock, A. M. Appel and J. C. Linehan, A Cobalt Hydride Catalyst for the Hydrogenation of CO_2: Pathways for Catalysis and Deactivation, *ACS Catal.*, 2014, **4**, 3755–3762.

30 T. Fogeron, T. K. Todorova, J. P. Porcher, M. Gomez-Mingot, L. M. Chamoreau, C. Mellot-Draznieks, Y. Li and M. Fontecave, A Bioinspired Nickel(Bis-Dithiolene) Complex as a Homogeneous Catalyst for Carbon Dioxide Electroreduction, *ACS Catal.*, 2018, **8**, 2030–2038.

31 R. Arévalo and P. J. Chirik, Enabling Two-Electron Pathways with Iron and Cobalt: From Ligand Design to Catalytic Applications, *J. Am. Chem. Soc.*, 2019, **141**(23), 9106–9123.

32 S. Dey, M. E. Ahmed and A. Dey, Activation of Co(I) State in a Cobalt-Dithiolato Catalyst for Selective and Efficient CO_2 Reduction to CO, *Inorg. Chem.*, 2018, **57**, 5939–5947.

33 (*a*) R. Jain, M. S. Mashuta, R. M. Buchanan and C. A. Grapperhaus, Electrocatalytic Hydrogen Evolution and Hydrogen Oxidation with a Ni$(PS)_2$ Complex, *Eur. J. Inorg. Chem.*, 2017, **2017**, 3714–3719; (*b*) A. Z. Haddad, D. Kumar, K. Ouch Sampson, A. M. Matzner, M. S. Mashuta and C. A. Grapperhaus, Proposed Ligand-Centered Electrocatalytic Hydrogen Evolution and Hydrogen Oxidation at a Noninnocent Mononuclear Metal-Thiolate, *J. Am. Chem. Soc.*, 2015, **137**, 9238–9241.

34 Y.-Y. Wu, J.-C. Hong, R.-F. Tsai, H.-R. Pan, B.-H. Huang, Y.-W. Chiang, G.-H. Lee, M.-J. Cheng and H.-F. Hsu, Ligand-Based Reactivity of Oxygenation and Alkylation in Cobalt Complexes Binding with (Thiolato)Phosphine Derivatives, *Inorg. Chem.*, 2020, **59**, 4650–4660.

35 B. M. Barry, B. W. Stein, C. A. Larsen, M. N. Wirtz, W. E. Geiger, R. Waterman and R. A. Kemp, Metal Complexes (M = Zn, Sn, and Pb) of 2-Phosphinobenzenethiolates: Insights into Ligand Folding and Hemilability, *Inorg. Chem.*, 2013, **52**, 9875–9884.

36 A. Chapovetsky, M. Welborn, J. M. Luna, R. Haiges, T. F. Miller and S. C. Marinescu, Pendant Hydrogen-Bond Donors in Cobalt Catalysts Independently Enhance CO_2 Reduction, *ACS Cent. Sci.*, 2018, **4**, 397–404.

37 (*a*) T. V. Russo, R. L. Martin and P. J. Hay, Application of Gradient-Corrected Density Functional Theory to the Structures and Thermochemistries of ScF_3, TiF_4, VF_5, and CrF_6, *J. Chem. Phys.*, 1995, **102**, 8023–8028; (*b*) Z. Li and W. Liu, Critical Assessment of TD-DFT for Excited States of Open-Shell Systems: I. Doublet-Doublet Transitions, *J. Chem. Theory Comput.*, 2016, **12**, 238–260.

38 C. Costentin, M. Robert and J. M. Savéant, Catalysis of the Electrochemical Reduction of Carbon Dioxide, *Chem. Soc. Rev.*, 2013, **42**, 2423–2436.

39 C. Costentin and J.-M. Savéant, Multielectron, Multistep Molecular Catalysis of Electrochemical Reactions: Benchmarking of Homogeneous Catalysts, *ChemElectroChem*, 2014, **1**, 1226–1236.

40 B. D. McCarthy, C. L. Donley and J. L. Dempsey, Electrode Initiated Proton-Coupled Electron Transfer to Promote Degradation of a Nickel(II) Coordination Complex, *Chem. Sci.*, 2015, **6**, 2827–2834.

41 (*a*) M. L. Clark, P. L. Cheung, M. Lessio, E. A. Carter and C. P. Kubiak, Kinetic and Mechanistic Effects of Bipyridine (Bpy) Substituent, Labile Ligand, and Brønsted Acid on Electrocatalytic CO_2 Reduction by Re(Bpy) Complexes, *ACS Catal.*, 2018, **8**, 2021–2029; (*b*) Y. Matsubara, D. C. Grills and Y. Kuwahara, Thermodynamic Aspects of Electrocatalytic CO_2 Reduction in Acetonitrile and with an Ionic Liquid as Solvent or Electrolyte, *ACS Catal.*, 2015, **5**, 6440–6452; (*c*) M. L. Pegis, J. A. Roberts, D. J. Wasylenko, E. A. Mader, A. M. Appel and J. M. Mayer, Standard Reduction Potentials for Oxygen and Carbon Dioxide Couples in Acetonitrile and N,N-Dimethylformamide, *Inorg. Chem.*, 2015, **54**, 11883–11888.